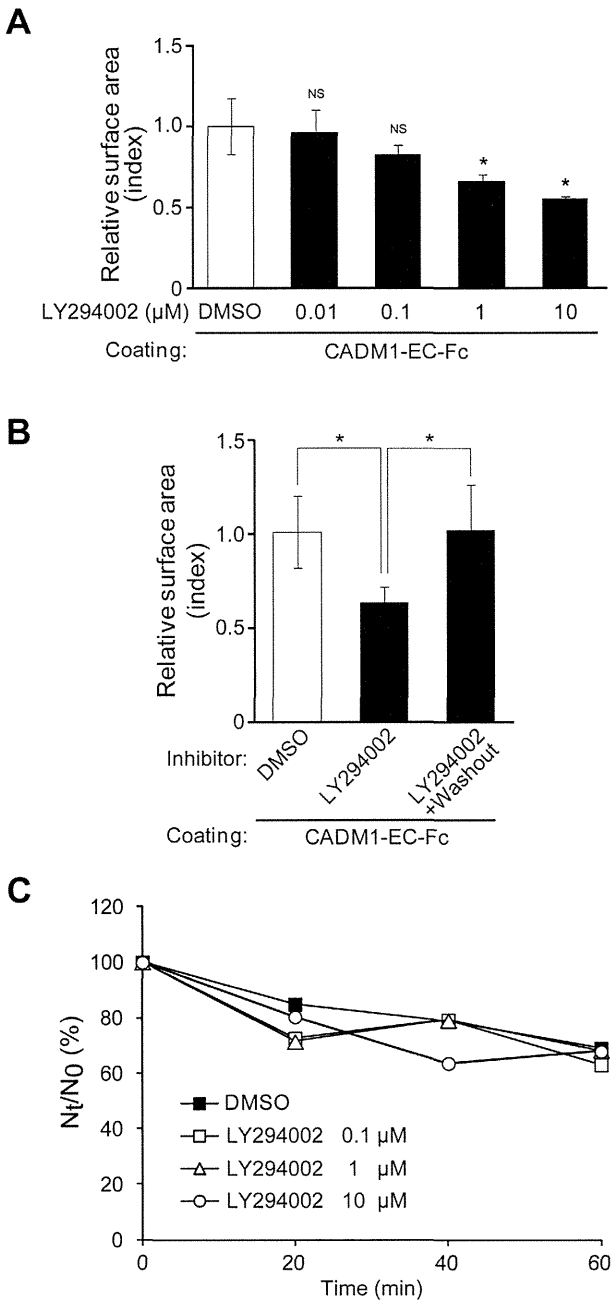

Figure 2. Two distinct inhibitors of PI3K suppress cell spreading mediated by *trans*-homophilic interaction of CADM1. (A) Cell spreading assay of MDCK+CADM1-GFP cells incubated on IgG or CADM1-EC-Fc in the presence of an inhibitor of PI3K, LY294002, from concentrations of 0.01 μM to 10 μM as indicated. *, $p<0.05$; NS, no significant difference (vs. cells on CADM1-EC-Fc with DMSO). (B) Cell spreading assay was performed using MDCK+CADM1-GFP cells cultured on CADM1-EC-Fc with 1 μM of LY294002 for 45 min and then washed and further incubated for 45 min in the presence of the same concentration of LY294002 (LY294002) or DMSO (LY294002+— washout). Representative images of CADM1-GFP are shown at the top of each bar graph. The area was normalized to that of cells on IgG with DMSO, and the relative value of the cell surface area to that of cells on CADM1-EC-Fc with DMSO was shown. *, $p<0.05$. (A and B) The results presented are mean ± SD of three independent experiments. More than 200 and 280 cells were counted in A and B, respectively. (C) Aggregation assay of MDCK+CADM1-GFP cells in Ca^{2+}- and Mg^{2+}-free condition in the presence of LY294002 at the concentrations indicated. The cell aggregation was represented by the ratio of the total particle number at time *t* of incubation (Nt) to the initial particle number (N0). The data shown here indicate the average Nt/N0 in triplicate experiments.
doi:10.1371/journal.pone.0082894.g002

the possible association of these molecules, MDCK+CADM1-GFP cells were used because MDCK cells expressed significant amounts of endogenous MPP3 and Dlg proteins. We examined whether CADM1 interacts with Dlg, a key molecule in connecting with PI3K *in vitro*. For this purpose, fused proteins of GST with the cytoplasmic fragment of CADM1 (GST-CADM1-C), a derivative of GST-CADM1-C lacking C-terminal 4 amino acids corresponding to PDZ-binding motif (GST-CADM1-CΔ4), as well as His-tagged N-terminal fragments of MPP3 (His-MPP3-N) and His-tagged N-terminal fragments of Dlg (His-Dlg-N), were constructed as shown in Fig. 4A. GST pull-down assay was then performed by incubating GST-CADM1-C or GST-CADM1-CΔ4 with His-MPP3-N and/or His-Dlg-N. Western blotting analysis revealed that His-Dlg-N was recovered with GST-CADM1-C depending on the presence of His-MPP3-N (Fig. 4B). On the other hand, neither His-Dlg-N nor His-MPP3 was bound to GST or GST-CADM1-CΔ4. These results indicate that MPP3 connects CADM1 with Dlg through direct binding of the N-terminal region of MPP3 with the class II PDZ-binding motif of CADM1 and with the N-terminal region of Dlg. Next, we examined possible *in vivo* complex formation of CADM1 with MPP3, Dlg, and p85. We first demonstrated that CADM1, MPP3, Dlg, and p85 were endogenously expressed in Caco-2 cells and co-localized one another at the cell-cell contact sites (Fig. 4C). When Caco-2 cells were transiently transfected with MPP3-HA and the lysates were immunoprecipitated with anti-CADM1 antibodies, signals corresponding to MPP3-HA and Dlg were detected by Western blotting using antibodies specific to HA and Dlg, respectively (Fig. 4D, left). MPP3-HA and p85 were also co-immunoprecipitated with Dlg in the same Caco-2 lysates that expressed MPP3-HA (Fig. 4D, right). Furthermore, when endogenous CADM1 expression in Caco-2 cells was depleted by transfection of shRNA of CADM1, localization of MPP3, Dlg, and p85 at plasma membrane was almost abrogated (Fig. S3). Moreover, the spreading of cells as well as the accumulations of a protein complex of GFP-Akt-PH, MPP3, Dlg, and p85 to the periphery of spreading cells were also impaired in MDCK cells expressing CADM1-ΔCT or MDCK cells expressing wild-type CADM1 together with siDlg (Fig. S4). These results suggest that CADM1 indirectly interacts with p85 by forming a multi-protein complex with MPP3 and Dlg and participates in cell spreading.

Discussion

CADM1 is expressed along the lateral membrane of epithelial cells and is involved in the attachment, formation, and maintenance of epithelial structure by forming a *trans*-homophilic interaction with CADM1 from adjacent epithelial cells. In the present study, to investigate signal transduction induced by CADM1-mediated intercellular adhesion, we established a cell-based assay to reconstitute an initial process of CADM1 interaction as cell spreading. The spreading of cells observed in the assay was specifically induced by *trans*-homophilic interaction of CADM1 because spreading was only observed when CADM1 was present both in the cell surface and on the glass and was abrogated by CADM1-blocking antibodies. By adding chemical inhibitors of known function in the assay and evaluating the degree of suppression in cell spreading through measuring the surface

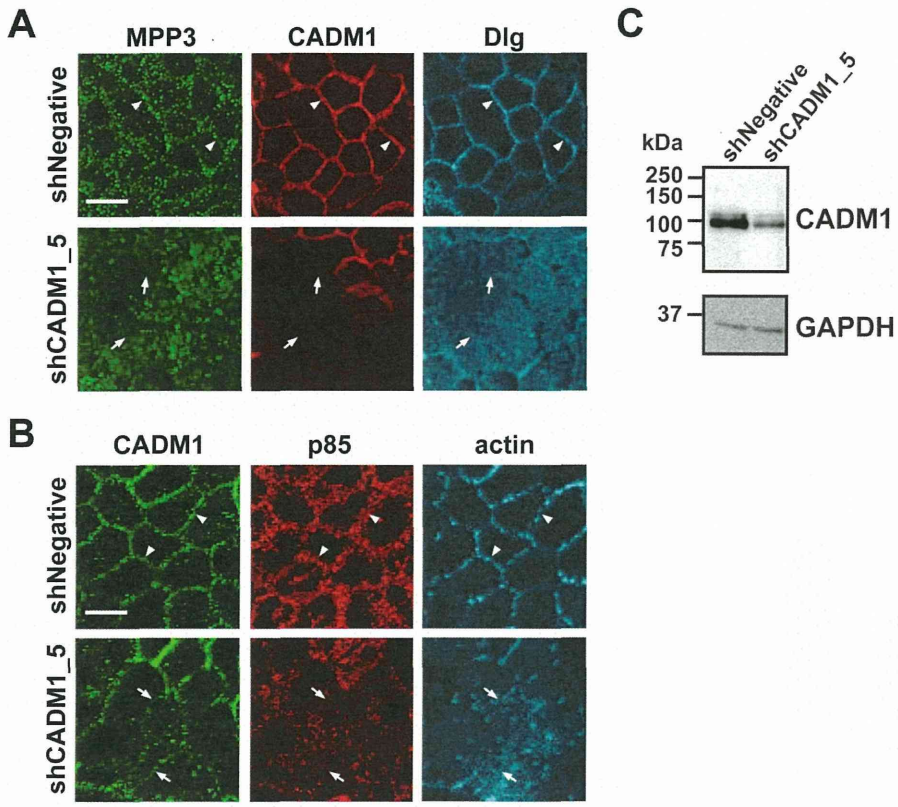

Figure 3. Activation of PI3K signaling is necessary for CADM1-mediated cell spreading. (A) MDCK cells stably expressing CADM1 were transiently transfected with GFP-Akt-PH and incubated on control IgG or CADM1-EC-Fc. Then, cells were visualized by staining with Alexa Fluor 568-labeled phalloidin. GFP-Akt-PH was observed at the periphery of the spreading cell where actin-rich lamellipodia were generated. High-magnification images of the region indicated by arrowhead were shown in the right panels. (B) Representative results of Western blotting analysis of phosphorylated-Akt, total Akt, and CADM1 using the lysates of MDCK+CADM1-GFP cells incubated on IgG or on CADM1-EC-Fc with DMSO (−) or with 10 μM of LY294002 (+). Note that the difference of signal intensities of Akt and p-Akt was due to the different sensitivities of antibodies and exposure time. The membrane was stained by Amido Black to confirm the equal loading of proteins. The amount of phosphorylated-Akt was normalized to that of the total Akt in each lane, and the relative value to cells on control IgG without LY294002 was calculated. The average scores of the relative values in 3 independent experiments are indicated in the lower panel. (C) MDCK+CADM1-GFP cells were incubated on control IgG or CADM1-EC-Fc in the presence of DMSO or 1 μM of the inhibitors of PI3K, Rac1 and/or Akt as indicated. The surface area was normalized to that of cells on IgG with DMSO, and the relative value to cells on CADM1-EC-Fc with DMSO was shown. The results presented are mean ± SD of five independent experiments. More than 470 cells were counted in the assay. *; $p<0.05$, **; $p<0.01$ (vs. cells on CADM1-EC-Fc with DMSO). #; $p<0.05$, NS; no significant difference (vs. cells on CADM1-EC-Fc with LY294002).
doi:10.1371/journal.pone.0082894.g003

area, signaling pathways activated by *trans*-homophilic interaction of CADM1 can be identified. Among 104 inhibitors screened in the assay, two independent inhibitors of PI3K, LY294002 and Wortmannin, suppressed the cell spreading most dramatically. The suppressor activity of LY294002 in cell spreading was reversible and dose-dependent. Furthermore, the cell spreading was reversibly inhibited by a PI3K inhibitor, LY294002, in a dose-dependent manner. Additionally, by visualizing the subcellular localization of PIP_3, a major product of PI3K, we demonstrated that PI3K was activated at the cell periphery where lamellipodia were generated. On the basis of these results, we speculate that CADM1 recruits PI3K to the cytoplasmic juxtamembrane domain to induce cell spreading. In addition to PI3K inhibitors, several known inhibitors showed partial activity in suppressing cell spreading. Some of them are related to PI3K signaling, like AKT or Rac1, while others appear to be independent of the PI3K pathways, which will be described elsewhere. MDCK cells were chosen in this assay because cell spreading was most dramatically and reproducibly observed in MDCK. In addition, we have previously demonstrated that MDCK cells transfected with a full length CADM1 showed suppressor effect in HGF-induced cell scattering in 2D-culture or tubulogenesis in 3D-culture but that transfection of CADM1ΔCT, CADM1 lacking 4.1-binding motif (CADM1Δ4.1BM), or CADM1 lacking PDZ-binding motif (CADM1ΔPDZBM) into MDCK lost the suppressor activity of scattering or tubulogenesis [27]. The functional significance of these molecules is then confirmed by transfecting shRNA of CADM1 or Dlg.

It has been demonstrated that CADM1 has potential to form heterophilic *trans*-interaction with other IgCAMs, such as CADM2/Necl-3, CADM3/Necl-1, Nectin-3, and CRTAM, depending on the types of cells [10,22]. Therefore, analyses of *trans*-heterophilic interactions of CADM1 with other molecules using similar cell-based assay would clarify different signaling pathways activated by specific types of cell adhesion.

Since the cytoplasmic domain of CADM1 was essential for cell spreading, we analyzed the intracellular pathways leading to activation of PI3K. On the basis of the following three pieces of evidence reported so far, we hypothesized that CADM1 would recruit PI3K through MAGuKs. (1) We, and others, showed that

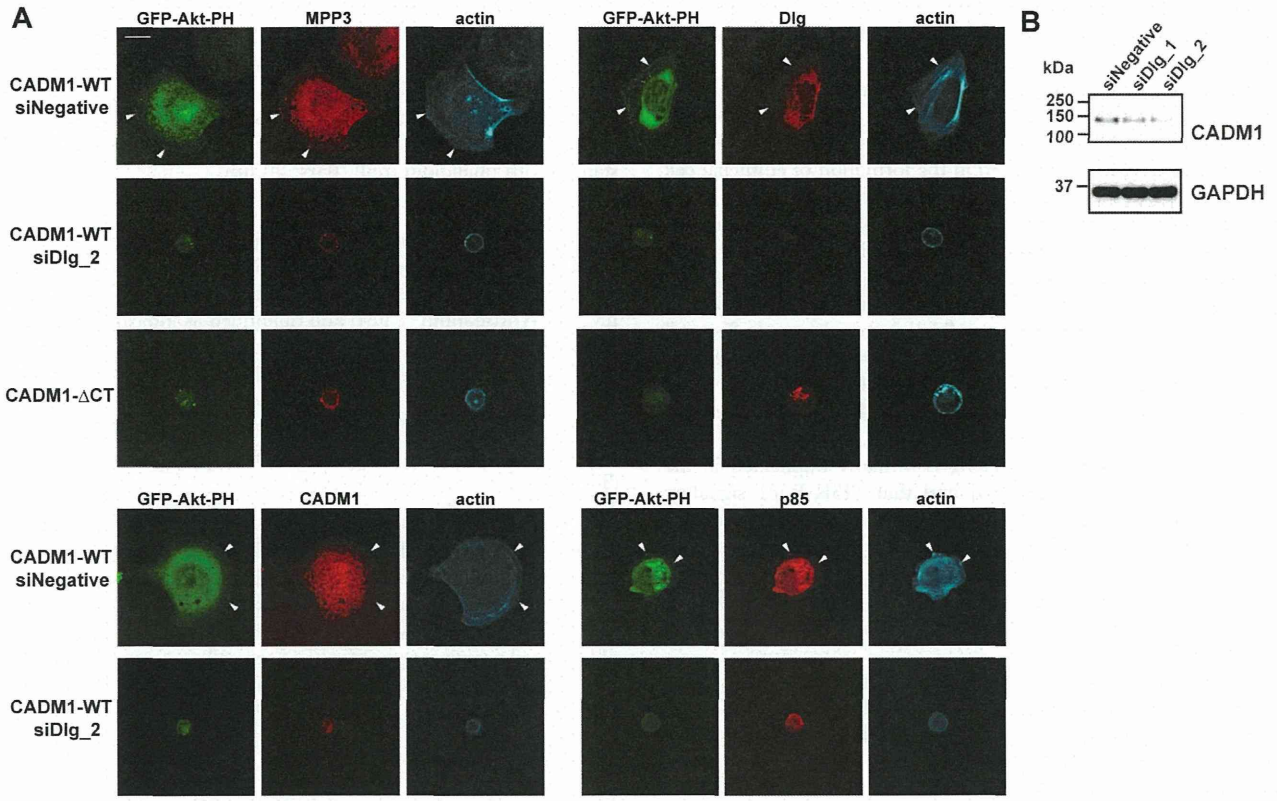

Figure 4. Membrane-associated guanylate kinase homologs (MAGuKs), MPP3 and Dlg, link CADM1 with p85 by forming a multi-protein complex. (A) Schematic representation of the structures of CADM1, MPP3, and Dlg proteins. In amino acid sequences of the cytoplasmic domain of CADM1, consensus sequences of 4.1- and class II PDZ-binding motifs are highlighted by grey and black, respectively. The GST-fusion protein of CADM1 with an entire cytoplasmic fragment (GST-CADM1-C) and a mutant form lacking a class II PDZ-binding motif (GST-CADM1- CΔ4) are schematically represented below. N-terminal fragments of MPP3 and Dlg were purified as His-fusion proteins and used for an *in vitro* binding assay. (B) Interaction of GST-CADM1 with His-MPP3 and/or His-Dlg was examined by GST pull-down assay. Binding proteins were detected by Western blotting using anti-His tag antibodies, whereas GST-fusion proteins were detected by staining the membrane with Coomassie Brilliant Blue (CBB). (C) Localization of CADM1, MPP3, Dlg, and p85 in confluent Caco-2 cells. Confluent Caco-2 cells were fixed and stained with anti-CADM1 antibodies (green) and anti-MPP3 (upper), anti-Dlg (middle), or anti-p85 (lower) antibodies (red). Merged images are shown in the right panel. Bars: 20 μm. (D) Lysates of Caco-2 cells expressing MPP3-HA were immunoprecipitated (IP) with control rabbit IgG and anti-CADM1 (left) or anti-Dlg (right) antibodies and analyzed by Western blotting with antibodies against HA, Dlg, p85, and CADM1, as indicated. Black arrowheads indicate signals found in both the input and immunoprecipitates, whereas white arrowheads indicate signals only found in the input. Asterisks show non-specific bands.
doi:10.1371/journal.pone.0082894.g004

CADM1 associates with MAGuKs, such as MPP1-3, CASK, and Pals-2, through its class II PDZ-binding domain in epithelial cells [8–11]. (2) The SH2 domain of p85 interacts with Dlg, one of the MAGuKs carrying class I PDZ domain, when tyrosine residues of Dlg were phosphorylated [20]. (3) Several MAGuKs, such as MPP2, MPP3, CASK, and Dlg, bind to one another through their N-terminal L27 domain [21]. In the present study, we have demonstrated that CADM1 interacts with Dlg through MPP3 at the class II PDZ-binding motif *in vitro* using GST pull-down assay (Fig. 4B). Furthermore, we have shown that MPP3 and Dlg are co-immunoprecipitated with CADM1, while MPP3 and p85 are co-immunoprecipitated with Dlg by immunoprecipitation assay *in vivo* (Fig. 4D). By fluorescence microscopy analysis, we have also confirmed that CADM1 is co-localized with MPP3, Dlg, and p85 at the cell periphery (Fig. 4), whereas the recruitment of this protein complex to the cell periphery is abrogated by depletion of CADM1 or Dlg (Fig. S3 and Fig. S4). Taken together, these 4 proteins–CADM1, MPP3, Dlg, and p85–appear to form a complex at the juxtamembrane portion at the cell periphery and play an important role in cell spreading.

Cell spreading assay also identified Akt and Rac1 as possible molecules downstream of PI3K signaling when activated by the *trans*-homophilic interaction of CADM1. Both Akt and Rac1 are molecules known to be downstream of PI3K [19,23] in various cells, and we demonstrated that both Akt- and Rac1- inhibitors suppress spreading of MDCK cells significantly. However, quantitative measurement shows that the degree of suppression in cell spreading by Akt- or Rac1- inhibitors is only partial in comparison with that by PI3K inhibitor. On the other hand, when both an Akt- and Rac1- inhibitors are added simultaneously, cell spreading was fully suppressed. These findings demonstrate that Akt and Rac-1 act in the downstream of PI3K, but act independently of each other and that cell spreading assay has a great advantage in analyzing signaling pathways for its quantitative feature. These findings would be supported by our previous finding that Rac1 is sustained to be activated by HGF treatment when MDCK cells were transfected with full length CADM1 [26]. These findings might also be corresponding to another previous report by ours that introduction of dominant negative Rac1 suppressed lamellipodia formation of ATL cells when cultured on fibroblast, although ATL cells are not the epithelial origin [27].

Taken together, we propose a possible signaling pathway triggered by the *trans*-homophilic interaction of CADM1, as shown in Figure S5.

Expression of CADM1 is down-regulated in various carcinomas, and it is widely accepted that CADM1 is a tumor suppressor through its cell adhesive property. We have previously demonstrated that CADM1 is involved in the formation of epithelial cell structure since suppression of CADM1 expression by RNAi abrogated epithelial structure, induced simple flat morphology of cells and inhibited the maturation of cell-cell adhesion [9]. PI3K has also emerged as a major regulator of the cytoskeleton and cell polarity [24]. It is quite interesting that inhibition of PI3K by LY294002 causes a reduction in cell height but does not affect cell adhesion activity in epithelial cells [25]. Our study also indicates that the inhibition of PI3K does not affect cell adhesion activity by *trans*-interaction of CADM1 but abrogates following cell spreading activity induced by cytoskeletal remodeling. Furthermore, it has been reported that Rac1 signaling is similarly implicated in the maintenance of cell height [25] and that PI3K-Rac1 signaling serves as a key regulator for inducing the extension of cell-cell contact zones [26]. Taken together, these findings suggest that *trans*-homophilic interaction of CADM1 acts as an initial trigger on the membrane for the formation and maintenance of epithelial cell structure by activating PI3K-Rac1 pathways to reorganize the actin cytoskeleton.

In this connection, it is noteworthy that we have previously reported that overexpression of CADM1 in MDCK cells suppresses hepatocyte growth factor (HGF)-induced epithelial-mesenchymal transition (EMT), which is a well-known phenomenon associated with cancer cell invasion and metastasis [27]. In CADM1 over-expressing cells, prolonged activation of Rac1 induced by CADM1 and its cytoplasmic binding proteins appeared to inhibit EMT induction by HGF through the retention of epithelial cell adhesion. Although we did not investigate the mechanism of Rac1 activation in the study, the MAGuK-PI3K pathway could be a candidate for activating Rac1 in cells over-expressing CADM1. Thus, CADM1 appears to act as a suppressor of cancer cell invasion and metastasis by its activity in the formation and maintenance of adhesion-based epithelial cell structure.

In this study, we have demonstrated that cell-based screening assay is an effective tool for identifying low-molecular-weight compounds that target signaling pathways mediated by *tarns*-homophilic interaction of CADM1. By screening known inhibitors that suppress cell spreading, we found that the PI3K pathway was specifically activated by *trans*-homophilic CADM1 interaction. The protein complex of CADM1-MPP3-Dlg appears to recruit PI3K to the juxtamembrane region to induce actin reorganization by activating Akt and Rac1. In conclusion, the PI3K pathway is crucial for the signals mediated by *trans*-homophilic CADM1 interaction to cytoplasm, leading to cytoskeletal remodeling and the formation and maintenance of epithelial structure.

Supporting Information

Figure S1 Establishment of cell spreading assay. (A) Representative images of cells analyzed by spreading assay shown in Fig. 1A. In each assay, 10 fields were imaged in duplicate and average area of cells were quantified by image J software. MDCK (a and b) and MDCK+CADM1-GFP (c and d) cells were put on IgG (a and c) or CADM1-EC-Fc (b and d), respectively, as indicated on top of images. Two fields of phalloidin-stained (a and b) and GFP (c and d) images are shown. Bars: 50 μm. (B, C, and E) Representative images of spreading assay shown in Fig. 1B (B), Fig. 1C (C), and Fig. 1E (E). Cells stained with phalloidin are shown. Bars: 50 μm. (D) Localization of CADM1-FL-YFP and -ΔCT-YFP in confluent MDCK cells. Confluent MDCK cells stably expressing CADM1-FL-YFP or -ΔCT-YFP were fixed and stained with phalloidin (red). Bars: 20 μm.
(TIF)

Figure S2 PI3K inhibitors suppress cell spreading mediated by *trans*-homophilic interaction of CADM1. (A) Cell spreading assay was performed with DMSO, LY294002 (1 μM), or Wortmannin (1 μM) and quantified as indicated in Fig. 1. The surface area was normalized to that of cells on IgG with DMSO, and the relative value to cells on CADM1-EC-Fc with DMSO is shown. (B, C and D) Representative images of spreading assay shown in Fig. 2A (B), Fig. 2B (C) and Fig. 3C (D). Cells stained with phalloidin are shown. Bars: 50 μm.
(TIF)

Figure S3 Localization of MPP3, Dlg, and p85 in Caco-2 cells depleted CADM1. (A and B) Immunofluorescence analysis of Caco-2 cells stably expressing shNegative or shCADM1_5 using antibodies indicated on top of images. Arrowheads and arrows show colocalization and mislocalization of indicated proteins, respectively, at cell-cell contact sites. Bars: 20 μm. (C) Immunoblot analysis of Caco-2 cells expressing shNegative or shCADM1_5 with anti-CADM1 and anti-GAPDH antibodies.
(TIF)

Figure S4 Localization of GFP-Akt-PH and the components of CADM1 complex in cell spreading assay. (A) Representative images of MDCK cells transfected with GFP-Akt-PH, CADM1-WT or ΔCT, and/or siNegative or siDlg_2 and analyzed by spreading assays indicated at the left side of images. Immunofluorescence analysis was performed using antibodies against MPP3, Dlg, CADM1, and p85 as indicated. Bars: 20 μm. (B) Immunoblot analysis of MDCK cells transiently tranefected with siNegative, siDlg_1, or siDlg_2.
(TIF)

Figure S5 Schematic representation of the signaling pathways mediated by *trans*-homophilic interaction of CADM1 to cell spreading. When attached on the glass coated with CADM1-EC-Fc (upper), CADM1-expressing cells activate PI3K through MPP3 and Dlg, induce actin reorganization, and show cell spreading (lower).
(TIF)

Methods S1 Expression vectors, Cell culture and transfection, Antibodies and reagents, Immunoprecipitation and Western blotting, and Cell aggregation assay.
(DOCX)

Acknowledgments

The authors express their gratitude to Dr. T. Akaike, Tokyo Institute of Technology for the pcDNA3.1-IgG-Fc vector.

Author Contributions

Conceived and designed the experiments: SM MSY YM. Performed the experiments: SM MSY TM. Analyzed the data: SM MSY. Wrote the paper: SM MSY YM.

References

1. Juliano RL (2002) Signal transduction by cell adhesion receptors and the cytoskeleton: functions of integrins, cadherins, selectins, and immunoglobulin-superfamily members. Annu Rev Pharmacol Toxicol 42: 283–323.
2. Cavallaro U, Christofori G (2004) Cell adhesion and signalling by cadherins and Ig-CAMs in cancer. Nat Rev Cancer 4: 118–132.
3. Doherty P, Walsh FS (1996) CAM-FGF receptor interactions: a model for axonal growth. Mol Cell Neurosci 8: 99–111.
4. Bienz M, Clevers H (2000) Linking colorectal cancer to Wnt signaling. Cell 103: 311–320.
5. Kuramochi M, Fukuhara H, Nobukuni T, Kanbe T, Maruyama T, et al. (2001) TSLC1 is a tumor-suppressor gene in human non-small-cell lung cancer. Nat Genet 27: 427–430.
6. Murakami Y (2005) Involvement of a cell adhesion molecule, TSLC1/IGSF4, in human oncogenesis. Cancer Sci 96: 543–552.
7. Yageta M, Kuramochi M, Masuda M, Fukami T, Fukuhara H, et al. (2002) Direct association of TSLC1 and DAL-1, two distinct tumor suppressor proteins in lung cancer. Cancer Res 62: 5129–5133.
8. Fukuhara H, Masuda M, Yageta M, Fukami T, Kuramochi M, et al. (2003) Association of a lung tumor suppressor TSLC1 with MPP3, a human homologue of Drosophila tumor suppressor Dlg. Oncogene 22: 6160–6165.
9. Sakurai-Yageta M, Masuda M, Tsuboi Y, Ito A, Murakami Y (2009) Tumor suppressor CADM1 is involved in epithelial cell structure. Biochem Biophys Res Commun 390: 977–982.
10. Shingai T, Ikeda W, Kakunaga S, Morimoto K, Takekuni K, et al. (2003) Implications of nectin-like molecule-2/IGSF4/RA175/SgIGSF/TSLC1/SynCAM1 in cell-cell adhesion and transmembrane protein localization in epithelial cells. J Biol Chem 278: 35421–35427.
11. Biederer T, Sara Y, Mozhayeva M, Atasoy D, Liu X, et al. (2002) SynCAM, a synaptic adhesion molecule that drives synapse assembly. Science 297: 1525–1531.
12. Dimitratos SD, Woods DF, Stathakis DG, Bryant PJ (1999) Signaling pathways are focused at specialized regions of the plasma membrane by scaffolding proteins of the MAGUK family. Bioessays 21: 912–921.
13. Zheng CY, Seabold GK, Horak M, Petralia RS (2011) MAGUKs, synaptic development, and synaptic plasticity. Neuroscientist 17: 493–512.
14. Wang D, You Y, Case SM, McAllister-Lucas LM, Wang L, et al. (2002) A requirement for CARMA1 in TCR-induced NF-kappa B activation. Nat Immunol 3: 830–835.
15. Weiger MC, Wang CC, Krajcovic M, Melvin AT, Rhoden JJ, et al. (2009) Spontaneous phosphoinositide 3-kinase signaling dynamics drive spreading and random migration of fibroblasts. J Cell Sci 122: 313–323.
16. Furuno T, Ito A, Koma Y, Watabe K, Yokozaki H, et al. (2005) The spermatogenic Ig superfamily/synaptic cell adhesion molecule mast-cell adhesion molecule promotes interaction with nerves. J Immunol 174: 6934–6942.
17. Watton SJ, Downward J (1999) Akt/PKB localisation and 3′ phosphoinositide generation at sites of epithelial cell-matrix and cell-cell interaction. Curr Biol 9: 433–436.
18. Qian Y, Corum L, Meng Q, Blenis J, Zheng JZ, et al. (2004) PI3K induced actin filament remodeling through Akt and p70S6K1: implication of essential role in cell migration. Am J Physiol Cell Physiol 286: C153–163.
19. Vivanco I, Sawyers CL (2002) The phosphatidylinositol 3-Kinase AKT pathway in human cancer. Nat Rev Cancer 2: 489–501.
20. Laprise P, Viel A, Rivard N (2004) Human homolog of disc-large is required for adherens junction assembly and differentiation of human intestinal epithelial cells. J Biol Chem 279: 10157–10166.
21. Karnak D, Lee S, Margolis B (2002) Identification of multiple binding partners for the amino-terminal domain of synapse-associated protein 97. J Biol Chem 277: 46730–46735.
22. Boles KS, Barchet W, Diacovo T, Cella M, Colonna M (2005) The tumor suppressor TSLC1/NECL-2 triggers NK-cell and CD8+ T-cell responses through the cell-surface receptor CRTAM. Blood 106: 779–786.
23. Wennstrom S, Hawkins P, Cooke F, Hara K, Yonezawa K, et al. (1994) Activation of phosphoinositide 3-kinase is required for PDGF-stimulated membrane ruffling. Curr Biol 4: 385–393.
24. Gassama-Diagne A, Yu W, ter Beest M, Martin-Belmonte F, Kierbel A, et al. (2006) Phosphatidylinositol-3,4,5-trisphosphate regulates the formation of the basolateral plasma membrane in epithelial cells. Nat Cell Biol 8: 963–970.
25. Jeanes A, Smutny M, Leerberg JM, Yap AS (2009) Phosphatidylinositol 3′-kinase signalling supports cell height in established epithelial monolayers. J Mol Histol 40: 395–405.
26. Kovacs EM, Ali RG, McCormack AJ, Yap AS (2002) E-cadherin homophilic ligation directly signals through Rac and phosphatidylinositol 3-kinase to regulate adhesive contacts. J Biol Chem 277: 6708–6718.
27. Masuda M, Kikuchi S, Maruyama T, Sakurai-Yageta M, Williams YN, et al. (2005) Tumor suppressor in lung cancer (TSLC)1 suppresses epithelial cell scattering and tubulogenesis. J Biol Chem 280: 42164–42171.

Cancer Science
The official journal of the Japanese Cancer Association JCA

Lung cancer with loss of BRG1/BRM, shows epithelial mesenchymal transition phenotype and distinct histologic and genetic features

Daisuke Matsubara,[1,2] Yuka Kishaba,[1] Shumpei Ishikawa,[3] Takashi Sakatani,[1] Sachiko Oguni,[1] Tomoko Tamura,[1] Hiroko Hoshino,[1] Yukihiko Sugiyama,[4] Shunsuke Endo,[5] Yoshinori Murakami,[2] Hiroyuki Aburatani,[6] Masashi Fukayama[3] and Toshiro Niki[1,7]

[1]Department of Integrative Pathology, Jichi Medical University, Shimotsuke, Tochigi; [2]Division of Molecular Pathology, Institute of Medical Science, The University of Tokyo, Minato-ku, Tokyo; [3]Department of Human Pathology, Graduate School of Medicine, The University of Tokyo, Bunkyo-ku, Tokyo; [4]Division of Pulmonary Medicine, Jichi Medical University, Tochigi; [5]Division of General Thoracic Surgery, Jichi Medical University, Shimotsuke, Tochigi; [6]Division of Genome Science, Research Center for Advanced Science and Technology, The University of Tokyo, Meguro-ku, Tokyo, Japan

(Received August 22, 2012/Revised October 30, 2012/Accepted November 6, 2012/Accepted manuscript online November 19, 2012/Article first published online January 4, 2013)

BRG1 and BRM, two core catalytic subunits in SWI/SNF chromatin remodeling complexes, have been suggested as tumor suppressors, yet their roles in carcinogenesis are unclear. Here, we present evidence that loss of BRG1 and BRM is involved in the progression of lung adenocarcinomas. Analysis of 15 lung cancer cell lines indicated that BRG1 mutations correlated with loss of BRG1 expression and that loss of BRG1 and BRM expression was frequent in E-cadherin-low and vimentin-high cell lines. Immunohistochemical analysis of 93 primary lung adenocarcinomas showed loss of BRG1 and BRM in 11 (12%) and 16 (17%) cases, respectively. Loss of expression of BRG1 and BRM was frequent in solid predominant adenocarcinomas and tumors with low thyroid transcription factor-1 (TTF-1, master regulator of lung) and low cytokeratin7 and E-cadherin (two markers for bronchial epithelial differentiation). Loss of BRG1 was correlated with the absence of lepidic growth patterns and was mutually exclusive of epidermal growth factor receptor (EGFR) mutations. In contrast, loss of BRM was found concomitant with lepidic growth patterns and EGFR mutations. Finally, we analyzed the publicly available dataset of 442 cases and found that loss of BRG1 and BRM was frequent in E-cadherin-low, TTF-1-low, and vimentin-high cases and correlated with poor prognosis. We conclude that loss of either or both BRG1 and BRM is involved in the progression of lung adenocarcinoma into solid predominant tumors with features of epithelial mesenchymal transition and loss of the bronchial epithelial phenotype. BRG1 loss was specifically involved in the progression of EGFR wild-type, but not EGFR-mutant tumors. (*Cancer Sci* 2013; 104: 266–273)

Lung cancer is the leading cause of cancer death in many developed countries, including the United States and Japan.[1,2] The identification of genetic abnormalities, such as epidermal growth factor receptor (EGFR) mutations, KRAS mutations, EML4–ALK translocation, and MET amplifications has revolutionized our understanding of the molecular mechanisms in lung cancer development.[3] However, it has become increasingly apparent that epigenetic alternations play equally important roles in tumorigenesis, and among them, chromatin remodeling factors have attracted much attention recently.[4] Indeed, identification of mutations of chromatin remodeling factors in cancer has been a major hot topic in the past 2 years.[5–8]

BRG1 and BRM, two core catalytic ATPase subunits in human SWI/SNF chromatin remodeling enzymes, have now emerged as bona fide tumor suppressor genes.[9–12] Inactivating mutations of BRG1 have been identified in 35% of non-small cell lung cancer cell lines and a subset of primary lung cancer.[9] In a mouse model of lung cancer, targeted knockout of BRG1 can affect tumor development.[10] In contrast to BRG1, mutations of BRM have rarely been identified and epigenetic silencing of BRM plays a contributory role in some cancers.[4,11] However, whether loss of BRG1 and BRM affects phenotype and differentiation of lung cancer cells remains unexplored. Furthermore, the previous studies were conducted before the discovery of EGFR mutations, and thus relationship between the EGFR status and loss of BRG1 and BRM is completely unknown.

We have recently demonstrated that lung adenocarcinoma could be classified into two groups based on the patterns of gene expression and genetic abnormalities; bronchial epithelial phenotype tumors and mesenchymal-like phenotype tumors.[13] "Bronchial epithelial phenotype" represents a group of lung adenocarcinomas with high expression of bronchial epithelial markers. This group includes thyroid transcription factor (TTF)-1 positive terminal respiratory unit (TRU) type[14] in addition to TTF-1 negative tumors with high expression of bronchial epithelial markers such as CK7 and MUC1, as detailed in our previous report.[13] Bronchial epithelial phenotype tumor exhibits high phosphorylation of EGFR and MET and frequent mutations or amplifications of EGFR, MET, and HER2. In contrast, mesenchymal-like phenotype tumors were characterized by the absence of the bronchial epithelial phenotype, triple-negative for TTF-1, MUC1, and CK7, showed no or little phosphorylation of EGFR and MET, no mutation or amplification of EGFR, MET, or HER2, and with features of epithelial mesenchymal transition (EMT), such as low E-cadherin and high FGFR1, vimentin, and ZEB1 expressions.[13] The absence of mutations or amplifications of EGFR, MET, or HER2 in mesenchymal-like phenotype tumors suggested to us that other genetic or epigenetic abnormalities may play a role in this group of tumors.

We now show in this paper that loss of expression of chromatin remodeling factors, BRG1 and BRM, correlated with features of mesenchymal-like phenotype with solid predominant histology. In particular, BRG1 loss occurred exclusively in EGFR wild-type tumors.

[7]To whom correspondence should be addressed.
E-mail: tniki@jichi.ac.jp

doi: 10.1111/cas.12065

Materials and Methods

Cell lines and medium. We used 19 non-small cell lung cancer (NSCLC) cell lines; 15 adenocarcinoma cell lines (H23, H358, H441, H522, H1395, H1648, H1650, H1703, H1795, H2087, HCC827, HCC4006, Calu3, A549, PC-3), three large cell carcinoma cell lines (H661, H1299, Lu65), and one adenosquamous cell line (H596). HCC827, H1650, H1975, PC-3, and HCC4006 were EGFR-mutated cell lines. The sources of the cell lines were described in our previous report.[13] All cell lines were maintained in RPMI1640 supplemented with 10% FCS, glutamine, and antibiotics in a humidified atmosphere with 5% CO_2 and 95% air.

Genetic and protein analysis of cell lines. The DNA, RNA, and cell lysates were prepared from cell lines by standard procedures. Experimental details of sequencing, copy number analyses, and Western blotting are given in Doc. S1. Antibodies used in western blot analysis were summarized in Table 1.

Patients and tumors. Tumor specimens were obtained from 93 patients who underwent lung cancer surgery at the Jichi medical university hospital during the period from October 2005 to June 2008. The demographic and clinicopathologic details of the patients and tumors are provided in Doc. S1.

Immunohistochemistry and evaluation. Formalin-fixed, paraffin-embedded tumor specimens were analyzed by immunohistochemistry using antibodies to BRG1, BRM, E-cadherin, cytokeratin 7, MUC1, TTF-1, p-EGF, and p-MET. The sources of antibodies, staining procedures, and methods of evaluation, are given in Doc. S1.

Mutation analyses of formalin-fixed, paraffin-embedded tissue sections. Details are shown in Doc. S1.

Bioinformatic analyses and statistics. Details are shown in Doc. S1.

Results

Characteristics of lung adenocarcinoma cell lines with loss of BRG1 and/or BRM. First, we used 15 lung cancer cell lines, for which the mutational status of BRG1 was known, to investigate the molecular features that may characterize lung adenocarcinoma cell lines with loss of BRG1. Of the 15 cell lines, six cell lines harbored BRG1 mutations and nine cell lines did not, according to previous literature,[9,11] and the Sanger COSMIC database (http://www.sanger.ac.uk/genetics/CGP/cosmic/).

Figure 1 summarizes (i) the genetic status of BRG1, EGFR, MET, HER2, BRAF, and KRAS (upper panel), (ii) gene level expressions of BRG1, BRM, TTF1, MUC1, CK7, E-cadherin, and vimentin (middle panel), and (iii) protein expression levels of BRG1, BRM, TTF1, MUC1, CK7, E-cadherin, and vimentin (lower panel) of the 15 cell lines (the microarray analysis data of 15 cell lines is located in Data S1). All six BRG1-mutated cell lines showed extreme loss of BRG1 at gene and protein levels, EMT features (low E-cadherin and high vimentin), and loss of bronchial epithelial markers (TTF-1, CK7, and MUC1). In contrast, the nine BRG1-wild type cell lines showed high expressions of BRG1, as well as high expressions of bronchial epithelial markers and E-cadherin and low expression of vimentin, at both gene and protein levels. As for gene abnormalities, BRG1-wild type cell lines showed gene abnormalities for EGFR, MET, HER2, BRAF, or KRAS, but BRG1 mutated cell lines showed no such genetic abnormalities, except for KRAS mutations.

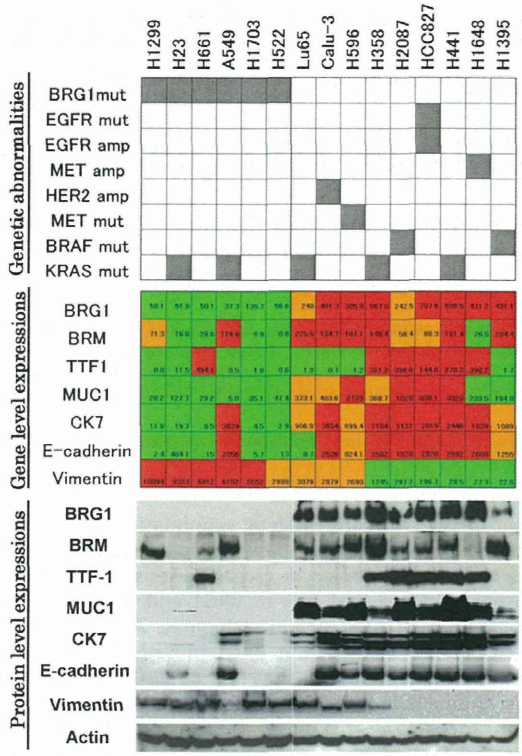

Fig. 1. Genetic status of BRG1, epidermal growth factor receptor (EGFR), MET, HER2, BRAF, and KRAS (upper panel), gene level expressions of BRG1, BRM, TTF1, MUC1, CK7, E-cadherin, and vimentin (middle panel), and protein expression levels of BRG1, BRM, TTF1, MUC1, CK7, E-cadherin, and vimentin (lower panel) of the 15 cell lines. In the upper panel, the grey box means presence of genetic abnormalities and the white box means absence of genetic abnormalities. Color indications in the middle lane are as follows: red means more than or equal to the average of each gene expression; orange: under the average and more than or equal to half the average; and green: under half the average.

We also examined the expressions of BRM in the same cell lines. Of the 15 cell lines, 10 cell lines expressed the BRM protein at modest or high levels, which was largely concordant

Table 1. Antibodies used in western blot analysis

Antibodies	Clone	Sources
BRG1 (sc-17796)	Mouse monoclonal	Santa Cruz Biotechnology (Santa Cruz, CA, USA)
BRM (A301-016A)	Rabbit polyclonal	Bethyl Laboratory (Montgomery, TX, USA)
TTF-1 (clone 8G7G3/1)	Mouse monoclonal	DAKO (Glostrup, Denmark)
Cytokeratin 7 (clone OV-TL 12/30)	Mouse monoclonal	DAKO (Glostrup, Denmark)
Vimentin (clon V9)	Mouse monoclonal	DAKO (Glostrup, Denmark)
E-cadherin (clone 36)	Mouse monoclonal	BD Biosciences (Franklin Lakes, NJ, USA)
MUC1 smaller cytoplasmic subunit	Hamster monoclonal	Lab Vision (Cheshire, UK)
Anti-rabbit IgG peroxidase conjugate		Amersham (Arlington Hights, IL, USA)
Anti-mouse IgG peroxidase conjugate		Amersham (Arlington Hights, IL, USA)
Anti-Armenian hamster IgG peroxidase conjugate		Jackson Immunoresearch (West Grove, PA, USA)

with gene expression (Fig. 1). As with BRG1, loss of BRM expression was similarly frequent in cell lines with EMT features and loss of the bronchial epithelial phenotype.

These results suggest the following: (i) loss of either or both BRG1 and BRM would be involved in the acquisition of EMT features and loss of the bronchial phenotype; and (ii) loss of BRG1 gene and protein expression correlate with the BRG1 mutation status.

We conducted the same analysis in five EGFR-mutated cell lines (HCC827, H1650, H1975, PC-3, and HCC4006), as shown in Figure S1. Although genetic status of BRG1 was unknown in H1650, H1975, PC-3, and HCC4006, all five EGFR-mutated cell lines showed high expression levels of BRG1, which suggested that loss of BRG1 would be mutually exclusive with EGFR mutations.

Immunohistochemical expression of BRG1 and BRM in primary lung adenocarcinoma tissues. Next, we used 93 cases of primary lung adenocarcinoma cases in our institution to examine the immunohistochemical expressions of BRG1 and BRM and their relationship with (i) histopathological subtypes, (ii) presence or absence of lepidic growth components, (iii) expressions of E-cadherin, TTF-1, CK7, and MUC1, (iv) genetic status of EGFR and KRAS, and (v) activation levels of EGFR and MET.

Overall, in the large majority of cases (>80%), nuclear staining for BRG1 and BRM was observed in cancer cells (Figs 2,3). Stromal cells constantly stained positive for BRG1 and BRM, and thus served as excellent internal positive controls. Using the criteria described in the Methods (Doc. S1), 11 cases (12%) were judged as showing low expression levels of BRG1 and 16 cases (17%) as showing low expression levels of BRM. Five cases (5%) showed low expression levels of both BRG1 and BRM. Most of the BRG1-low cases were either completely negative or showed only scattered positive staining for BRG1. In contrast, BRM showed a more heterogeneous staining pattern, typically showing strong positive staining in lepidic growth components, while showing negative or weak staining in invasive high-grade components (Fig. 4A–C).

Table 2 shows correlations between the expression levels of BRG1 and BRM and histopathological subtypes. All cases of well differentiated adenocarcinomas, that is, adenocarcinoma *in situ* (AIS) and minimally invasive adenocarcinoma (MIA), showed positive immunostaining for both BRG1 and BRM (20 of 20, 100%; Figs 2A,3A). Moderately differentiated adenocarcinomas, that is, acinar or papillary adenocarcinoma, also frequently showed positive immunostaining for both BRG1 and BRM (37 of 46, 80%; Figs 2B,3B), while some of them showed loss of either BRG1 or BRM (9 of 46, 20%; Figs 2D,3D). In contrast to these well- to moderately-differentiated tumors, poorly-differentiated adenocarcinomas (solid adenocarcinomas) frequently showed loss of expression of either BRG1 or BRM (12 of 13, 92%; Figs 2C,3C). Most cases (4 of 5, 80%) with loss of both BRG1 and BRM showed solid morphology (Table 2). One of three cases (33%) of invasive mucinous adenocarcinoma showed loss of BRG1.

We also examined correlations between the expression levels of BRG1 and BRM and the presence or absence of lepidic growth components (Table 3). Strikingly, all cases with BRG1 loss were devoid of lepidic growth components, while 6 of 16 cases with BRM loss showed lepidic growth components (Table 3).

Table 4 shows correlations between the expression levels of BRG1 and BRM and that of bronchial epithelial markers (TTF-1, CK7, and, MUC1) and E-cadherin. The expressions of TTF-1, CK7, MUC1 (membranous expression), and E-cadherin were frequently reduced in cases with loss of BRG1 and BRM (shown in Fig. S2). In particular, loss of E-cadherin and TTF-1 was remarkably correlated with loss of BRG1; all but one case of E-cadherin-low tumors showed BRG1 loss and all cases with BRG1 loss showed low expression levels of TTF-1. Depolarized expression of MUC1 was also frequent in cases with loss of BRG1 and BRM.

Table 4 also shows correlations between the expression levels of BRG1 and BRM and genetic status of EGFR and KRAS. Mutually exclusive correlations were observed between EGFR mutations and BRG1 loss ($P = 0.0006$), but no significant correlations between EGFR mutations and BRM loss ($P = 0.3382$). KRAS mutations were sometimes harbored by cases with loss of BRG1 or BRM.

We also examined the expressions of phospho-EGFR and phospho-MET and compared them with the expressions of BRG1 and BRM (Table 4). Low phosphorylation levels of EGFR were significantly correlated with loss of BRG1 and BRM ($P = 0.0003$, $P < 0.0001$, respectively). Phosphorylation

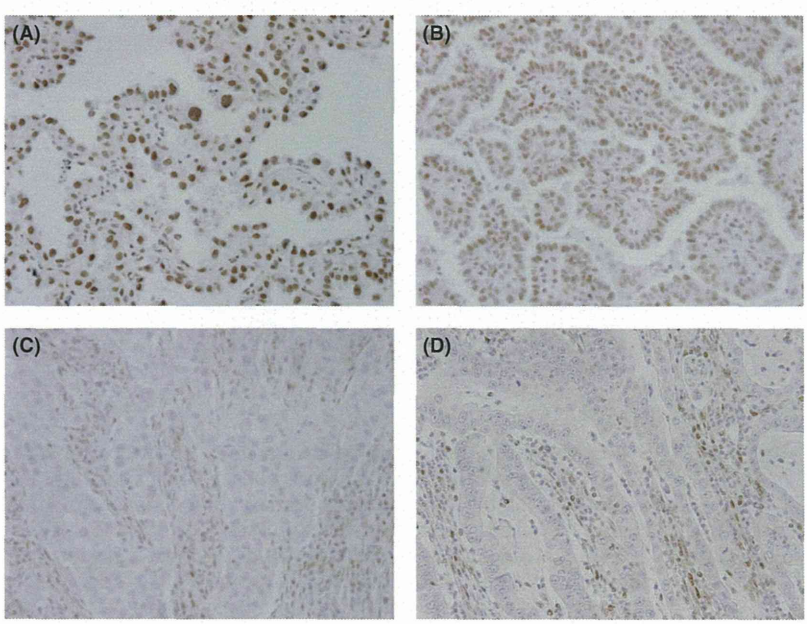

Fig. 2. BRG1 expressions in lung adenocarcinomas. Overall, more than 80% of cases showed positivity for BRG1. (A) Lepidic growth components showed strong immunoreactivity for BRG1. (B) Moderately differentiated adenocarcinomas, such as papillary adenocarcinoma, frequently showed positivity for BRG1. (C) Solid adenocarcinomas with mucin were frequently negatively stained for BRG1. (D) Some cases with papillary or acinar morphology showed negative staining for BRG1. Note BRG1 positivity in stromal cells.

doi: 10.1111/cas.12065

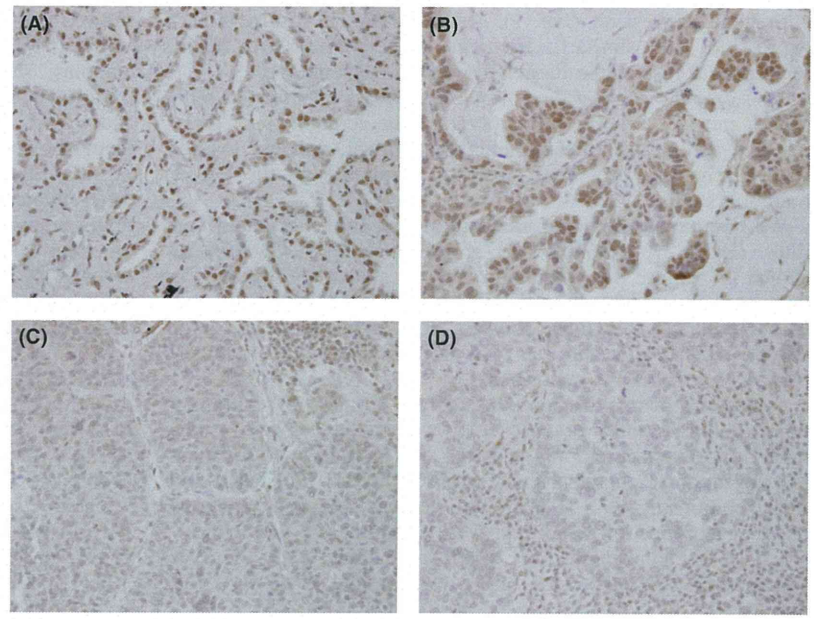

Fig. 3. BRM expressions in lung adenocarcinomas. Overall, more than 80% of cases showed positivity for BRM. (A) Lepidic growth components showed strong immunoreactivity for BRM. (B) Moderately differentiated adenocarcinomas, such as papillary adenocarcinoma, also often show positivity for BRM. (C) Solid adenocarcinoma with mucin frequently showed negative or weak staining for BRM. (D) Some cases with papillary or acinar morphology show negative staining for BRM. Note BRM positivity in stromal cells.

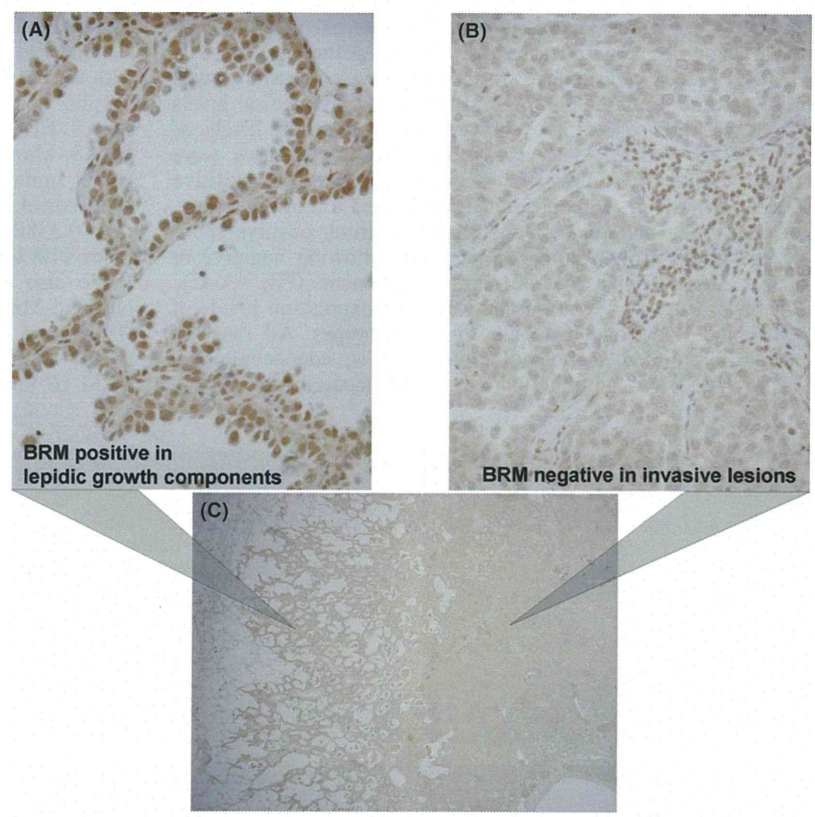

Fig. 4. Heterogeneous BRM expression in lung adenocarcinoma. (A) High-power field of lepidic growth components, which show strong positivity for BRM. (B) High-power field of invasive acinar components, which show negative positivity for BRM. (C) Low-power field of invasive adenocarcinoma with lepidic growth components; left side shows lepidic growth components, and right side shows invasive acinar components.

of MET tended to be low in cases with loss of BRG1 and BRM, but the difference was not significant.

BRM loss was significantly more frequent in heavy smokers and in cases with vessel invasion ($P = 0.0093$ and $P = 0.0002$, respectively; Table 3). BRG1 loss was significantly correlated with pleural invasion and pleural dissemination ($P = 0.0471$ and $P = 0.0449$, respectively; Table 3).

Prognostic significance of the expressions of BRG1 and BRM. Lastly, we performed hierarchical cluster analysis using the publicly available data of 442 primary lung adenocarcinoma cases,[15] based on the gene expressions of BRG1, BRM, TTF-1, MUC1, CK7, E-cadherin, and vimentin. Results are shown in Figure 5(A). Principally, primary lung adenocarcinoma cases could be classified into two groups: (i) tumors

Table 2. Correlations between expression levels of BRG1 and BRM and histopathological subtypes of primary lung adenocarcinomas

	BRG1 high BRM high	BRG1 low BRM high	BRG1 high BRM low	BRG1 low BRM low	Total
Non-mucinous adenocarcinoma *in situ*	8	0	0	0	8
Minimally invasive adenocarcinoma	12	0	0	0	12
Invasive adenocarcinoma, lepidic predominant	9	0	0	0	9
Invasive adenocarcinoma, acinar predominant	8	0	2	1	11
Invasive adenocarcinoma, papillary predominant	29	3	3	0	35
Invasive mucinous adenocarcinoma	2	1	0	0	3
Colloid adenocarcinoma	1	0	0	0	1
Invasive adenocarcinoma, micropapillary predominant	1	0	0	0	1
Invasive adenocarcinoma, solid predominant	1	2	6	4	13
Total	71	6	11	5	93

Table 3. Correlations between expression levels of BRG1 and BRM and clinico-pathological factors

	BRG1 expression			BRM expression		
	High	Low	*P*-value	High	Low	*P*-value
Pathological stage						
I	60	7	0.5082	57	10	0.3499
II + III + IV	22	4		20	6	
T-stage						
T1	52	5	0.2508	48	9	0.6492
T2, T3, T4	30	6		29	7	
Nodal involvement†						
Positive	20	1	0.3608	17	4	0.7381
Negative	61	8		58	11	
Lymphatic invasion						
Positive	22	1	0.2004	18	5	0.5066
Negative	60	10		59	11	
Vessel invasion						
Positive	23	5	0.2373	17	11	0.0002
Negative	59	6		60	5	
Pleural invasion						
Positive	21	6	0.0471	21	6	0.4122
Negative	61	5		56	10	
Dissemination						
Positive	3	2	0.0449	4	1	0.8648
Negative	79	9		73	15	
Pulmonary metastasis						
Positive	4	0	0.4540	4	0	0.3514
Negative	78	11		73	16	
Lepidic growth						
Present	65	0	<0.0019	59	6	0.0019
Absent	17	11		18	10	
Smoking Index						
≤ 600	26	6	0. 1344	22	10	0.0093
>600	56	5		55	6	

†Pathological N-factors were not determined for three cases of stage IV patients with pleural dissemination. Underlined values are $P < 0.05$.

Table 4. Correlations between expression levels of BRG1 and BRM and genetic status of EGFR and KRAS and expression levels of E-cadherin, TTF-1, CK7, MUC1, phopsho-MET, and phospho-EGFR

	BRG1 expression			BRM expression		
	High	Low	*P*-value	High	Low	*P*-value
EGFR mutations						
Positive	45	0	0.0006	39	6	0.3382
Negative	37	11		38	10	
KRAS mutations						
Posivite	5	2	0.1537	4	3	0.0615
Negative	77	9		73	13	
E-cadherin						
High	81	3	<0.0001	72	12	0.0227
Low	1	8		5	4	
TTF-1						
High	62	0	<0.0001	57	5	0.0010
Low	20	11		20	11	
CK7						
High	74	4	<0.0001	67	11	0.0707
Low	8	7		10	5	
MUC1(membranous)						
High	63	3	0.0007	62	4	<0.0001
Low	19	8		15	12	
MUC1(depolarized)						
High	7	3	0.0596	4	6	0.0001
Low	79	8		73	10	
Phospho-EGFR						
High	69	4	0.0003	67	6	<0.0001
Low	13	7		10	10	
Phospho-MET						
High	19	2	0.7102	19	2	0.2892
Low	63	9		28	14	

Underlined values are $P < 0.05$.

showing high expression levels of TTF-1, MUC1 and E-cadherin, and low expression levels of vimentin, and (ii) tumors showing low expression levels of TTF-1, MUC1 and E-cadherin, and high expression levels of vimentin (Fig. 5A). High expression levels of both BRG1 and BRM were frequently seen in the former, while low expression levels of either of or both BRG1 and BRM were frequently seen in the latter (Fig. 5A). These results confirm and reinforce data from cancer cell lines and primary lung adenocarcinoma cases in our institution.

To ascertain the prognostic significance of the expressions of BRG1 and BRM in lung adenocarcinoma, we undertook a survival analysis using the Kaplan–Meier method. We separated 442 lung adenocarcinoma cases into three groups based on the gene expression levels of BRG1 and BRM; (i) cases with high expression (more than or equal to the average); (ii) cases with moderate expression (under the average, and more than or equal to half the average); and (iii) cases with low expression (under half the average). Results are shown in Figure 5(B). High expression of BRG1 and BRM both correlated significantly with better prognosis. Figure 5(C) also shows patient survival curves for the four groups: (i) BRG1-high and BRM-high; (ii) BRG1-high and BRM-low; (iii) BRG1-low and BRM-high; and (iv) BRG1-low and BRM-low. The BRG1-low and BRM-low group showed significantly poorer prognosis than the other groups.

doi: 10.1111/cas.12065